ELSEVIER

Journal of Structural Geology 28 (2006) 1316–1326

JOURNAL OF STRUCTURAL GEOLOGY

www.elsevier.com/locate/jsg

Influence of deflection on a fold-to-fault progression: field evidence from near Marietta, South Carolina

C.W. Clendenin [a,*], J.M. Garihan [b]

[a] South Carolina Department of Natural Resources, Geological Survey, 5 Geology Road, Columbia, SC 29212, USA
[b] Furman University, Department of Earth and Environmental Sciences, Greenville, SC 29613, USA

Received 14 January 2005; received in revised form 2 December 2005; accepted 5 December 2005
Available online 19 May 2006

Abstract

Four periods of deformation (D1–D4) are recognized in the Lion Park Road borrow pit near Marietta, South Carolina. Although each period is characterized by distinct structures, D3 produced two structural styles (D3a, D3b) resulting from layer-parallel shortening. D3a is characterized by detachment folding at the tip of an underlying thrust. D3b is a fold-to-fault progression that was localized by east-dipping, quartz-filled gash fractures. The fold-to-fault progression demonstrates the influence of a mechanical anisotropy on ramp development.

The early stages of D3b were formed by deflection of northwest-directed, layer-parallel shortening and active, down-section propagation of folds and thrusts. Following connection with a splay of basal detachment, later D3b stages resulted from up-section movement that produced kink folding and a throughgoing thrust. This up-section movement deformed and modified the geometries of older, down-section structures. Detailed mesoscopic field observations, integrated with a combination of current thrust fault models, are used to interpret the D3b fold-to-fault progression.

Keywords: Deflection; Folding; Thrust faulting; Progression of deformation; Fault-propagation folding

1. Introduction

During his mapping of Cleveland 7.5-minute quadrangle, Greenville and Pickens Counties, South Carolina, Garihan (2000) recognized polyphase deformation in an active borrow pit near Marietta, South Carolina (Fig. 1). It was re-examined and described as part of the South Carolina Geological Survey Piedmont Reconnaissance Project, focusing on the identification of structural styles in the Inner Piedmont (Clendenin and Garihan, 2004). Overprinting relations show that four deformation periods (D1–D4) are preserved in the multilayered metamorphic rock sequence. The structures developed during two deformation periods are assigned to specific regional events: D1 recumbent isoclines are related to the Early Paleozoic Taconic emplacement of the Six Mile Nappe (Griffin, 1974), and D4 left-oblique faults are part of the Mesozoic oblique extension (Garihan et al., 1990). The D2 and D3 compressive structures are presumed related to the Acadian and Alleghanian orogenies, respectively.

Both D2 and D3 include ductile and brittle structural styles as part of their deformational progression (Clendenin and Garihan, 2004). D2 structural styles evolved from symmetric upright folds to moderately inclined close folds to thrust faults that unfolded D1 and D2 fold limbs. Unfolding was the result of translation along the thrust that shallowed the interlimb angle. D3 produced two structural styles (D3a, D3b). D3a is characterized by west-vergent, gently inclined detachment folds (Fig. 2). Folds and thrusts localized by east-dipping, quartz-filled gash fractures (referred to here as gash fractures) characterize D3b. The two styles are assigned to the same deformation period because both folded older D2 thrusts prior to D4 oblique-slip offset.

Both D3a and D3b were products of layer-parallel shortening (Clendenin and Garihan, 2004). The recognition of D3a detachment folding was important in our interpretation of D3b structures. The rounded fold form of the D3a detachment folds (Fig. 2) implies that progressive kink folding was inhibited (Erslev and Mayborn, 1997), while the asymmetric character of the fold suggests that it tightened in response to continued shortening (Homza and Wallace, 1997). In detachment fold evolution, initial shortening is taken up by layer-parallel shortening above a detachment (Homza and Wallace, 1997). Moreover, layer-parallel shortening precedes or is simultaneous with the propagation of the basal detachment

* Corresponding author.
E-mail address: clendenin@dnr.state.sc.us (C.W. Clendenin).

0191-8141/$ - see front matter © 2006 Elsevier Ltd. All rights reserved.
doi:10.1016/j.jsg.2005.12.005

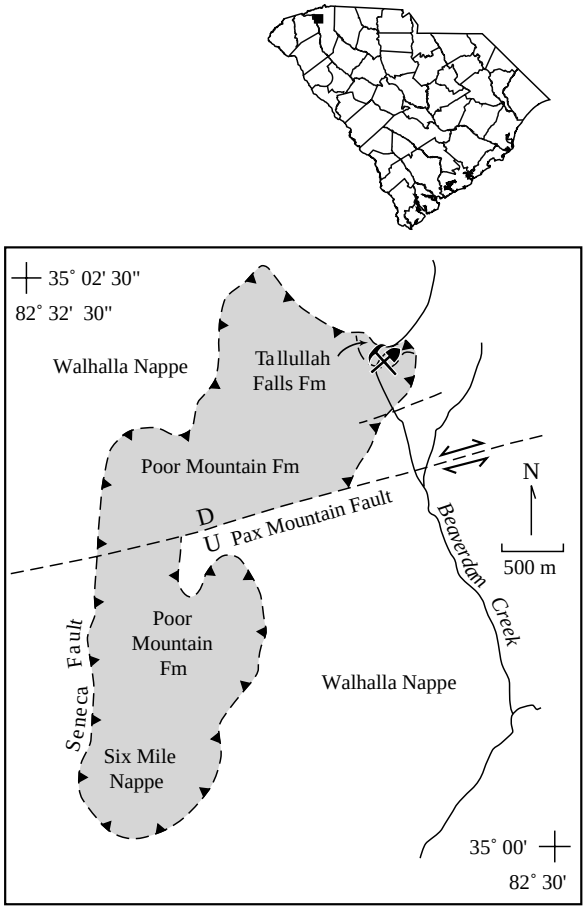

Fig. 1. Generalized geology map of the southeast part of Cleveland 7.5-minute quadrangle, Greenville County, South Carolina (modified after Garihan, 2000).

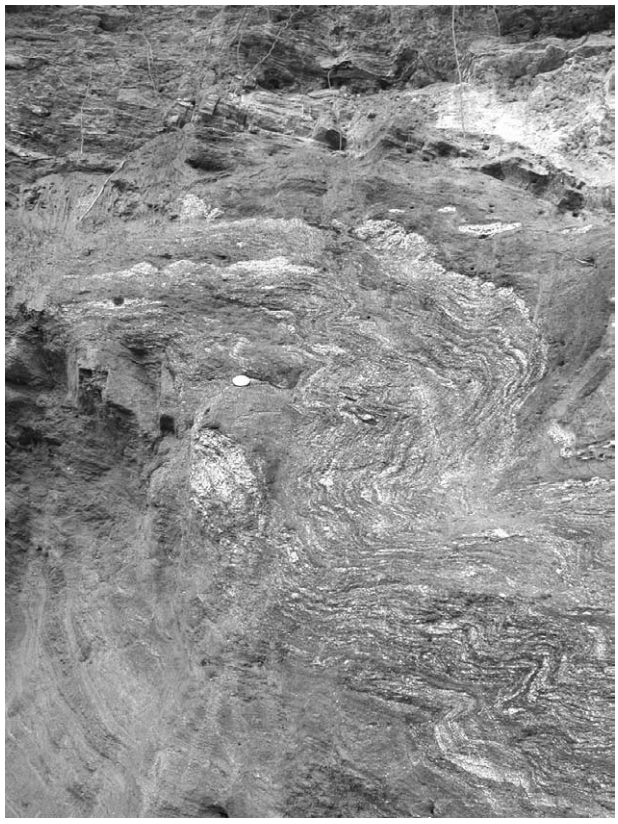

Fig. 2. D3a detachment fold preserved in south wall of borrow pit. Coin is approximately 4 cm, and view is to the south-southeast.

(Koyi et al., 2004). Although a basal detachment was not exposed in the Marietta borrow pit, the development of fold–fault structures and the presence of upward-ramping imbricates were taken to indicate the presence of a basal detachment below the borrow pit floor.

Layer-parallel shortening was considered to be similar to shear-related flow. The nucleation of shear-related folds can be achieved only by the onset of local or general perturbations in flow (Carreras et al., 2005). Carreras et al. (2005) further suggested that shear-related folds can result from the presence of rigid objects, from mechanically heterogeneous foliated rocks, from competency contrast between layers, or from variation in layer thickness. Therefore, any pre-existing mechanical anisotropies encountered by layer-parallel shortening should have a controlling influence on subsequent structural development above a basal detachment in the Marietta borrow pit.

2. Observations at the Lions Park Road borrow pit

The Lions Park Road borrow pit is an elongate, north–south cut that exposes an east view of the geology of a hill above Beaverdam Creek. The cut is approximately 60 m long; at the 30 m position, it is 9 m high. Small north and south views are scattered along the length of the cut where material has been extracted perpendicular to the hill slope.

In the cut, mining has exposed an interlayered sequence of psammitic gneiss, mica schist, migmatitic schist, amphibolite, and minor biotite gneiss. This sequence is part of the upper Tallalah Falls Formation that crops out over a limited area in the northeast corner of a klippe of the Six Mile Nappe (Garihan, 2000; Fig. 1). Regionally, the klippe is deformed by east- and south-plunging folds and by the Pax Mountain fault.

The geology in the cut is described in detail in Clendenin and Garihan (2004). Observations were described in a north–south direction and were located spatially by measurements from a continuous tape stretched along the length of the cut. At 32 m south of the north end of the cut, D3b structures are exposed in a south view of a small bench that was left in front of the borrow-pit face (Fig. 3), and in an eastward extension of that view that we had dug. In the bench, a sequence of mica schist, migmatitic schist, and amphibolite is exposed vertically. In the eastward extension, a similar multilayer sequence is exposed with interlayers of psammitic gneiss. At the west end of the bench, lithologic contacts are abrupt and subhorizontal. Such relations suggest simple interlayering of rock units versus structural juxtaposition.

The middle migmatitic schist layer is unique because it contains gash fractures. The geometry, location, and en échelon character of the gash fractures suggest that they formed on a fold limb. We considered the gash fractures to be kinematic

Fig. 3. Bench in front of borrow pit face. D3b deformation stages identified in the bench are labeled. Coin is approximately 4 cm, and view is to the south.

indicators of D2 flexural-slip folding. Where the bench meets the borrow-pit face, a northwest-vergent D2 thrust cuts up through the migmatitic schist layer from the underlying mica schist contact (Fig. 4). In both the north and south ends of the borrow-pit, D2 thrusts have unfolded fold limbs (Clendenin and Garihan, 2004); unfolding resulted from translation along the thrust that shallowed the interlimb angle. On the basis of these observations, we interpret the gash factures to have formed on a forelimb of a D2 fold, and that their present orientation was the result of unfolding by the recognized D2 thrust (Clendenin and Garihan, 2004).

After a small fault-propagation fold was exposed where the bench met the original borrow pit's face, the entire bench was uncovered and washed (Fig. 3). Three other structures were preserved in the bench. All four structures were localized by gash fractures. The recognition of those structures prompted the excavation of an eastward extension (referred to here as extension), where another structure was exposed. After observing the five structures, we concluded that up- and down-section changes in the profile of an antiform–synform pair and presence or absence of thrusting in each of the structures marked stages in a progression of deformation

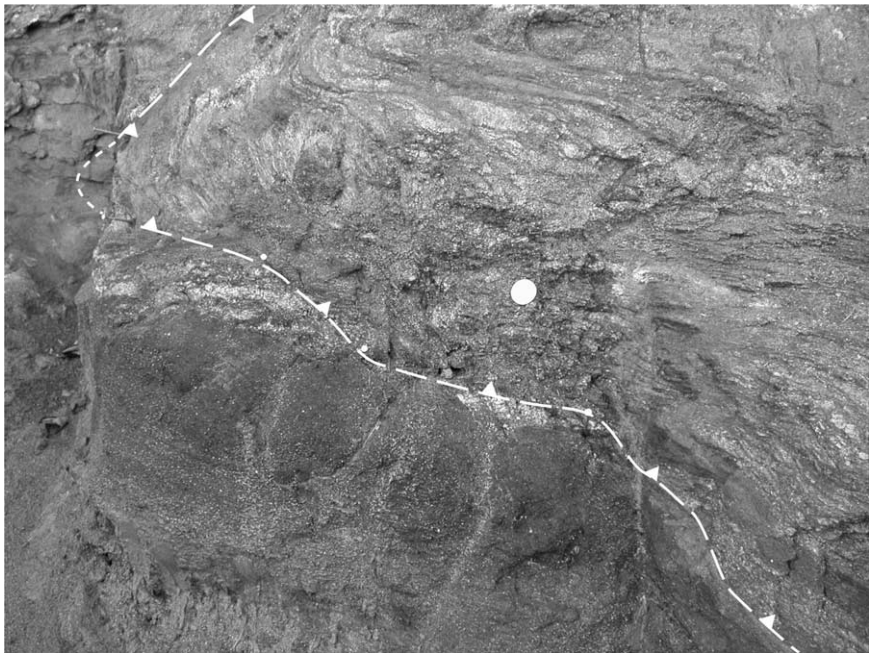

Fig. 4. Northwest-vergent D2 thrust where bench meets the borrow pit face. Coin is approximately 4 cm, and view is to the south-southeast.

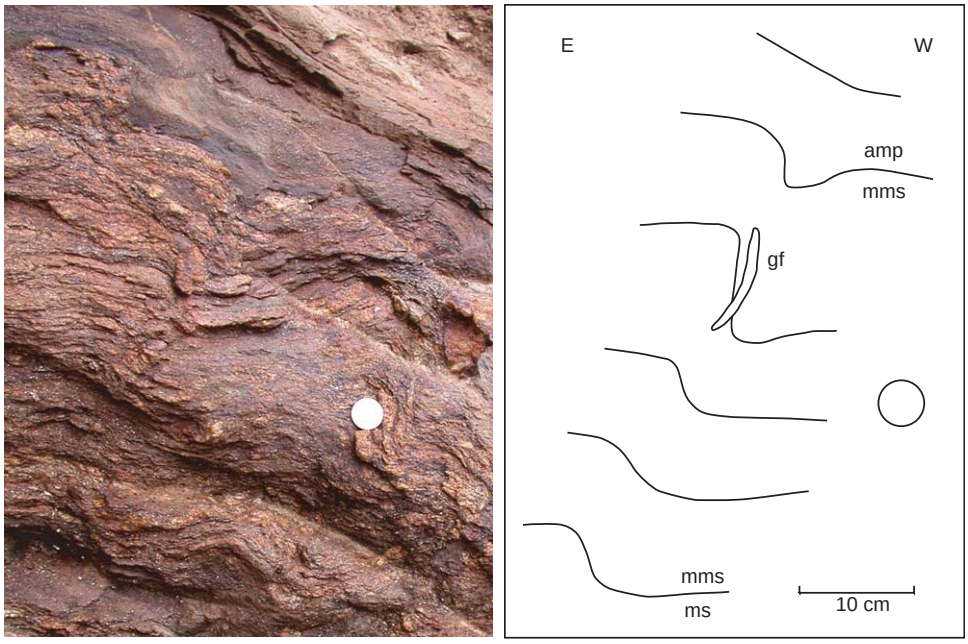

Fig. 5. B1: Stage 1 in deformation progression. Structure represents initial deflection at quartz-filled gash fracture heterogeneity. Line drawing is provided to complement descriptions in text. Coin is approximately 4 cm, and view is to the south.

(Clendenin and Garihan, 2004). The following structural observations were made; the B designation stands for D3b and the number represents the stage.

B-1: B-1 is the least developed of the five structures (Fig. 5). Adjacent to the gash fracture, the overlying amphibolite–migmatitic schist contact is folded into an asymmetric, moderately inclined, gentle antiform. Antiformal warping is minimal below the gash fracture. Across the gash fracture, migmatitic schist layers are folded more tightly into a moderately to steeply inclined, open synform. Synformal warping extends downward to the underlying migmatitic schist–mica schist contact. No fault planes are present.

B-2: B-2 shows that an amplification of folding occurred after the B-1 stage (Fig. 6). The overlying amphibolite–migmatitic schist contact has been folded into a west-vergent, gently inclined, open antiform. The overlying contact in the hinge zone of this antiform is 10 cm higher than the same contact adjacent to the gash fracture. Increased layer thicknesses in

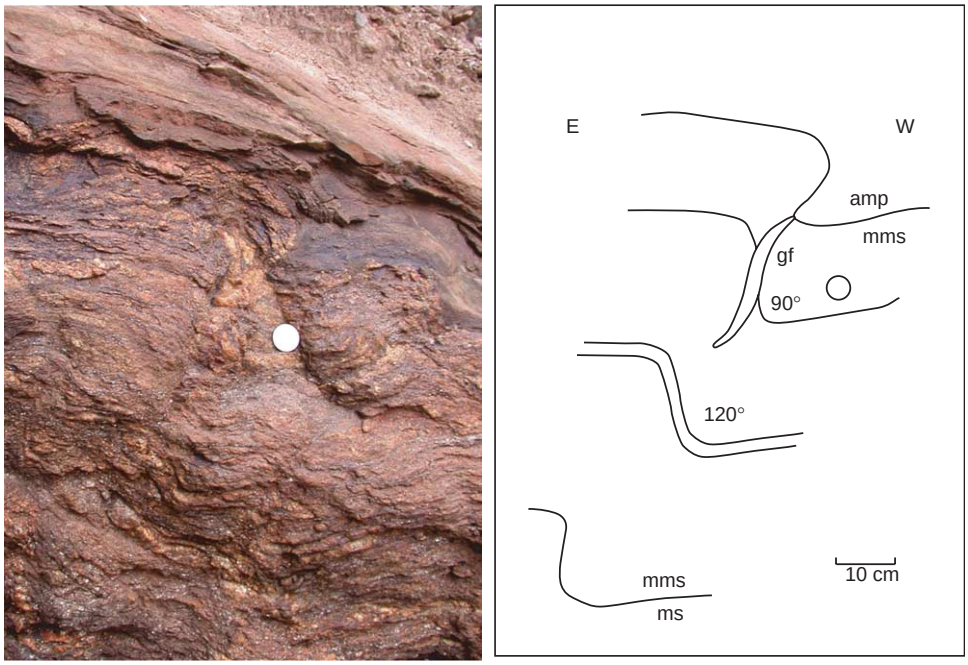

Fig. 6. B2: Stage 2 in deformation progression. Continued deflection at the quartz-filled gash fracture heterogeneity results in an antiform–synform pair. Line drawing is provided to complement descriptions in text. Coin is approximately 4 cm, and view is to the south.

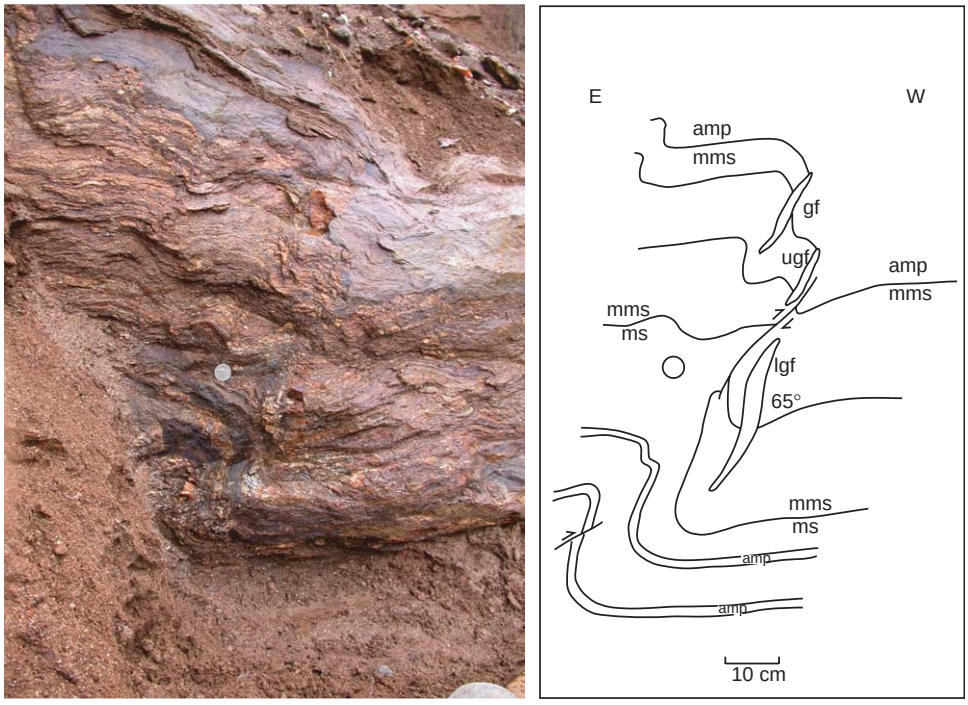

Fig. 7. B3: Stage 3 in progression of deformation. Faulting adjacent to heterogeneity determines location of ramp. Footwall synform is distinct and is not faulted during this stage of development. Line drawing is provided to complement descriptions in text. Coin is approximately 4 cm, and view is to the south.

the antiform indicate that schist has moved into the fold nose. Downward toward the underlying migmatitic schist–mica schist contact, migmatitic schist layering is subhorizontal.

At the upper tip of the gash fracture, an asymmetric, gently to moderately inclined, close synform folds the overlying amphibolite–migmatitic schist contact (Fig. 6). Here, the east-dipping, overturned limb is the shorter limb. Downward and adjacent to the gash fracture, the synform has an asymmetric, moderately inclined, open profile and an interlimb angle of 90°. West-dipping layers adjacent to the gash fracture also are thinned. Below the gash fracture, the synform is symmetric, moderately inclined, and gentle to open with an interlimb angle of 120°. Synformal folding warps the underlying migmatitic schist–mica schist contact and D2 fault downward 15 cm. No fault planes are visible.

B-3: B-3 is centered on the lower and larger of an en échelon pair of gash fractures (Fig. 7). The lower gash fracture is cut by a 40° E-dipping fault plane; reverse offset is visible on the fault that lies on the west side of upper gash fracture segment (upper segment). The overlying amphibolite–migmatitic schist contact has moved up along the fault, and the underlying migmatitic schist is juxtaposed to the overlying amphibolite across the fault. At the end of the upper segment, the amphibolite is deformed into a gently inclined open antiform. Downward and adjacent to the faulted upper segment, the antiform has a west-vergent, asymmetric close profile. Migmatitic schist layers in the forelimb are thinned.

Below the upper segment, the underlying migmatitic schist–mica schist contact also has moved up-to-the west (reverse) 20 cm relative to the contact in the footwall and is juxtaposed to migmatitic schist across the fault. The fault plane also separates the upper segment from the lower gash fracture segment (lower segment) (Fig. 7), where migmatitic schist layers are deformed into a moderately inclined, asymmetric, close synform. The synform has an interlimb angle of 65°, and its asymmetric east limb ends abruptly against the thrust which now lies on the east side the lower segment.

Adjacent to the fault in the hanging wall, the lower migmatitic schist–mica schist contact is generally subhorizontal, and the underlying mica schist layer is thickened (Fig. 7). An upright, symmetric antiform is developed 15 cm east of the fault along the contact. Below the contact, mica schist with thin interlayers of amphibolite is folded into a gently inclined, open antiform–synform pair (with an interlimb angle of approximately 90°). The axial surface of the antiform is concave upward, and some thickening has occurred in the synform trough near the tip of the lower segment. The tip of a small thrust, dipping 5° E, cuts through the forelimb of the antiform just above the trough of its paired synform.

B-4: B-4 was exposed in the south wall of the extension (Fig. 8). An open synform with an interlimb angle of 110° overlies the D2 thrust. This synform has an east-dipping, moderately inclined axial surface and is outlined by a layer of psammitic gneiss that ends abruptly at the upper surface of the thrust. Slickenlines mark psammitic gneiss layer boundaries on both limbs of the synform. Eastward into the extension, the axial surface of the synform is gently inclined, and the fold has an interlimb angle of 90°.

A west-vergent, recumbent, close to open antiform is present 15 cm above the previously described synform. A larger antiform with a chevron profile can be seen folding all of

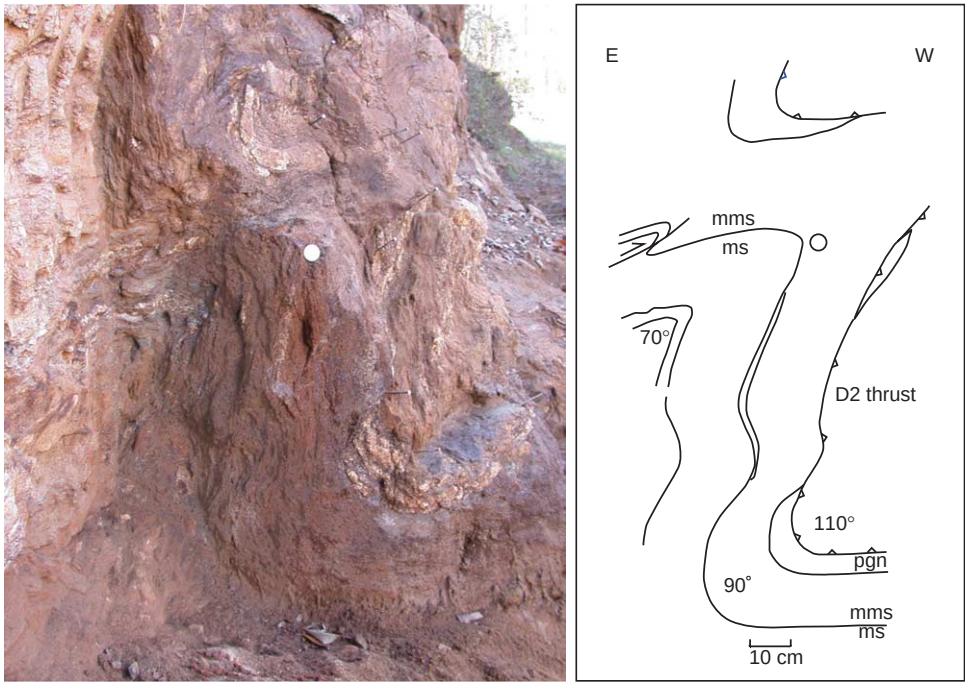

Fig. 8. B4: Stage 4 in progression of deformation. Development of kink fold prior to propagation of throughgoing fault. Nails mark folded D2 thrust. Line drawing is provided to complement descriptions in text. Coin is approximately 4 cm, and view is to the south.

the layers above the recumbent antiform, as well as the D2 thrust (Fig. 8). This chevron fold has an interlimb angle of 70°, and only a short segment of its backlimb exposed in the extension. Slickenlines mark forelimb and backlimb layer boundaries. A west-vergent, subhorizontal (~10° E) thrust cuts through the chevron from its backlimb and offsets both the psammitic layer and D2 thrust approximately 5 cm west. Where the extension ends, the profile of the chevron fold is moderately inclined and close with an interlimb angle of 65°.

When the psammitic gneiss layer is traced in the south wall, appearances suggest that the chevron fold is paired with the previously described underlying synform (Fig. 8). The profiles of the two folds, however, are different. The chevron fold has an angular hinge and a planar axial surface. The synform has a rounded hinge zone, and its profile is concave upward. The chevron fold form suggests that subsequent modification may have occurred because paired antiforms in the first three stages have rounded crests.

B-5: B-5 is located where the bench meets the original borrow pit face (Figs. 3 and 9). The overlying amphibolite–migmatitic schist contact is folded into a west-vergent, moderately inclined, angular, open antiform with an interlimb angle of 100°. This antiform is broken by a fault. The backlimb of the antiform is subhorizontal, and an east-dipping gash fracture marks the faulted hinge zone of the fold. The underlying migmatitic schist–mica schist contact is folded into a west-vergent, moderately inclined, close antiform that is chevron shaped and has an interlimb angle of 58°. This antiform's overturned, east-dipping forelimb is juxtaposed to the fault and the east-dipping gash fracture. The antiform's backlimb also is subhorizontal as defined by the underlying migmatitic schist–mica schist contact.

In the footwall of the fault, the overlying amphibolite–migmatitic schist contact dips 70° W, and the contact is folded into a gentle synform with an angular trough (Fig. 9). Below the contact, an open synform is present. Migmatitic schist layers in the short east limb dip 80° or more to the west and end abruptly at the thrust. Adjacent to the lower part of the gash fracture, the synform has an asymmetric, east-dipping, moderately inclined, close profile. Migmatitic schist layers in the short east limb are thinned. Across the gash fracture, thrusting juxtaposes mica schist (east side) and migmatitic schist (west side). Below the lower gash fracture, the synform has a more gently inclined, close profile, and the shorter east limb again ends abruptly at the thrust. Near the bottom of the bench, only half of the trough and west limb of the synform are preserved where the throughgoing thrust steps out of the mica schist layer and offsets a folded D2 thrust.

The B-5 thrust juxtaposes the underlying mica schist layer (east side) and the migmatitic schist layer (west side) where the thrust ramps into subparallelism with the east-dipping, lower gash fracture (Fig. 9). The thrust appears to flatten into parallelism with east-dipping, upper gash fracture at the overlying amphibolite contact. Displacement on the thrust decreases upward from 40 cm on the underlying migmatitic schist–mica schist contact to 8 cm on the overlying amphibolite–migmatitic schist contact. The entire structure has the structural style of a fault-propagation fold.

3. Thrust models

The classic ramp and thrust model of thrust nucleation, developed on observations of the Pine Mountain thrust

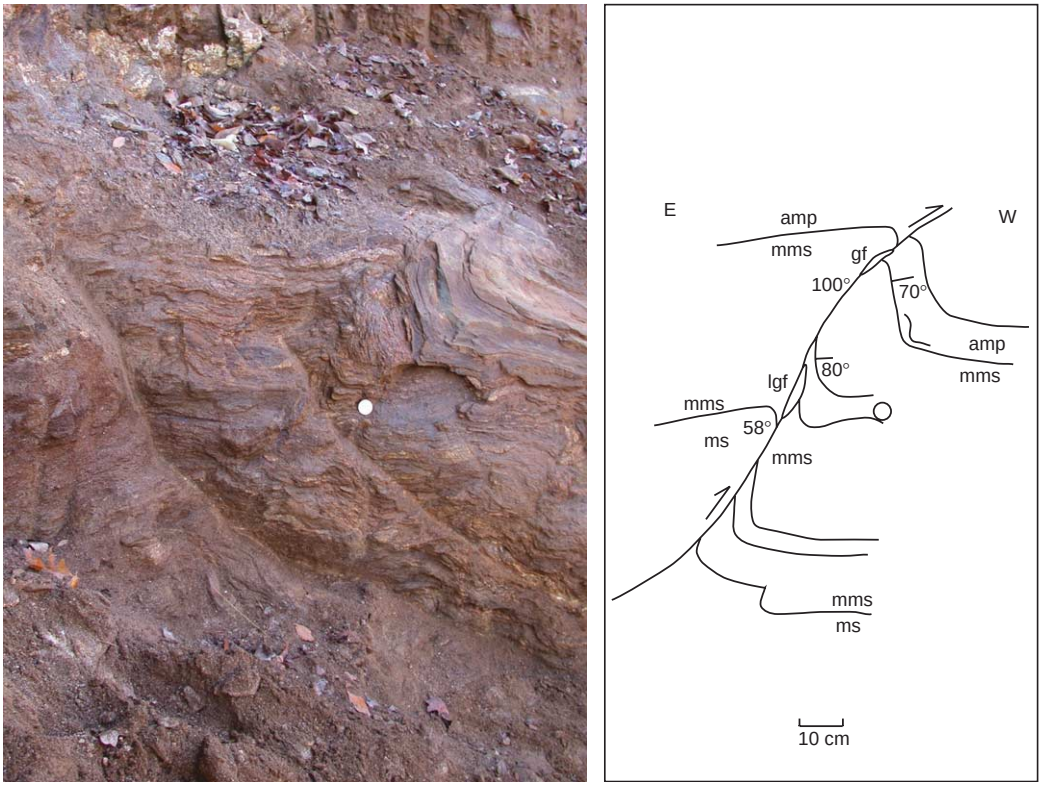

Fig. 9. B5: Stage 5 in progression of deformation. Throughgoing fault overprints early fold-dominated structures to develop structural style. Line drawing is provided to complement descriptions in text. Coin is approximately 4 cm, and view is to the south.

(Rich, 1934), connected rheologic properties with thrust style. Rich (1934) envisioned that thrusts nucleated in a deeper incompetent bed; as layer-parallel shortening continued, frictional resistance increased as the faulting process moved material in the incompetent bed (a flat) in the tectonic transport direction. When resistance became too great, the thrust tip cut up-section through overlying competent layers (a ramp) until it could step into another incompetent bed (Rich, 1934). Eisenstadt and DePaor (1987) proposed that thrusts nucleate in competent layers at shallow depths because deeper, underlying layers cannot move until brittle cover fails. Failure of competent layers caused initial slip on ramps, which, in turn, created tension in the adjacent underlying layering, leading to failure. Fault movement, thus, is both up- and down-section away from the nucleation point. When two propagating fault tips meet in an underlying incompetent layer, the faults merge in a fashion similar to stream capture (Eisenstadt and DePaor, 1987). When the two models are compared, the primary differences are: (1) how the mechanical properties of a multilayered sequence react to imposed compressive stress; (2) where the thrust nucleates; (3) what direction, or directions, faulting propagates; and (4) when the ramp and flat style developed.

Both thrust models are supported by experiments. Centrifuge models show thrust-ramp nucleation at the base of a competent layer and only upward propagation (Dixon and Liu, 1992; Liu and Dixon, 1995, and references therein). In high-resolution scaled sandbox models, Storti et al. (1997) documented thrust-ramp nucleation in the middle of a multilayer sequence and both up- and down-section propagation. The down-section propagation of the fault tip was faster than up-section propagation because the amount of deformation is greater in the lower part of the multilayer sequence (Storti et al., 1997). In an analysis of different size thrust faults, Ellis and Dunlap (1988) also have pointed out that thrust faults nucleate and develop above the main décollement, propagate both up- and down-section toward a flat, and do not step up from a basal décollement. To bridge the gap between these basal-nucleation and middle-nucleation models, Morley (1994) suggested that, after the thrust propagates to the basal décollement, a new structural style might be superimposed on the original one. After the fault's connection with the basal décollement (detachment), the evolution of the structure is controlled by upward movement on the larger throughgoing fault (Mitra, 2002).

4. Discussion

Our observations indicated that the intensity of deformation varies markedly adjacent to the different gash fracture in terms of amplification of folds and presence of faulting. Differences were interpreted to represent a structural progression development during D3b deformation (Fig. 10). We also consider the progression to be field evidence addressing the primary differences between the conceptual thrust models because the direction, or directions, that faulting propagated can be deciphered.

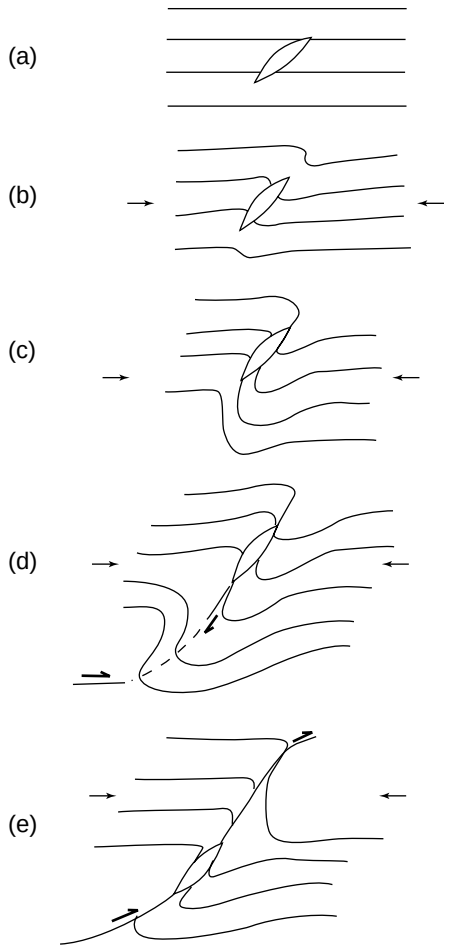

Fig. 10. Generalized stages of D3b progression of deformation. (a) Quartz-filled gash fracture is present in interlayered rock sequence before application of layer-parallel shortening. (b) Gash fracture acts as heterogeneity and disrupts imposed layer-parallel shortening. (c) Active down-section propagation of footwall synform results as layer-parallel shortening continues. (d) Initial faulting is adjacent to gash fracture. Ramp is localized as faulting migrates downward toward lower detachment. (e) Upward movement on throughgoing fault dominates final stages of structural development.

4.1. Early stages of development (B-1–B-3)

A basic premise in the experiments of Dixon and Liu (1992), Storti et al. (1997), and Koyi et al. (2004) was that layer-parallel shortening affected the materials during the application of compressive stress. During any given deformation period, such layer-parallel shortening would be in the tectonic transport direction of the compressive stress field. Moreover, strength heterogeneities, flaws, or other anisotropies capable of concentrating stress affect a layer's mechanical properties during shortening (Bump, 2003) and control resulting strain (Homza and Wallace, 1997). Overprinting relations at a mechanical anisotropy may produce folds during progressive deformation (Passchier and Trouw, 1998; Carreras et al., 2005).

The subparallelism of the amphibolite–migmatitic schist–mica schist layers away from the gash fractures implies that the interlayered rocks were strain-transmitting units with a relatively high intrinsic competency. Buckling of migmatitic schist layers adjacent to the B-1 gash fracture indicates that the gash fractures are mechanical anisotropies in the otherwise continuous migmatitic schist layer (Figs. 6 and 10a). The development of an antiform–synform pair adjacent to the gash fracture early in the B-series progression (Fig. 7) shows that such mechanical anisotropies act as barriers to layer-parallel shortening and that such anisotropies are nucleation sites for deformation (Bump, 2003).

During B-1, an antiform–synform pair formed prior to faulting as folding propagated up- and down-section as a result of deflection of layer-parallel shortening (Fig. 6). Down-section propagation indicates that the footwall was an unconstrained participant. Synformal folding to the underlying migmatic schist–mica schist contact also indicates that fold growth was more active down-section away from anisotropy (Fig. 10c).

In B-1 and B-2, deflection-driven folding adjacent to the gash fracture initiated as open folds (Figs. 7 and 10c). Antiformal folding dies out a short distance below the gash fracture, whereas synformal folding was more active. The synform's axial surface extends downward to the underlying migmatitic schist–mica schist contact. In mechanical models of fault-related folds with unconstrained footwalls, asymmetric synclines do develop (Cooke and Pollard, 1997). Ramsay (1992) has argued that, apart from conventional thinking, footwall rocks with more or less the same mechanical properties as hanging wall rocks can deform more actively. Experiments support Ramsay's argument and show that deformation will proceed at a faster rate down-section than up-section at corresponding stages of development (Storti et al., 1997). Such an asymmetric distribution of deformation rates results from the amount of strain being greater in the lower part of the sequence (Storti et al., 1997). In general, B1 and B2 fold relations confirm that deflection-driven folding develops at different rates adjacent to an anisotropy and that the synform is the more active of the fold pair in early deformation stages (Fig. 10b and c).

In B-3, synformal profiles became more asymmetric as they tightened during progressive deformation (Figs. 8 and 10d). A thrust also nucleated adjacent to the gash fracture and propagated up- and down-section cutting the gash fracture. B3 footwall relations offer an explanation of thrust nucleation. Migmatitic schist layers in the steeply dipping limb of the footwall synform adjacent to the gash fracture are thinned and appear stretched. In fault-propagation folds, Alonso and Teixell (1992) suggest that thinning and stretching are the product of heterogeneous strain (pure shear thrust-parallel stretch and simple shear) superimposed on flexural mechanisms. This interpretation appears applicable because footwall synclines look like inverted fault-propagation folds and fault ramps may propagate down-section (McConnell et al., 1997). During progressive deformation, a thrust nucleates at the point of highest strain (cf. Alonso and Teixell, 1992). Strain rate was amplified by the high-competency contract between the gash fracture and the stretched migmatitic schist layers, and failure leads to thrusting (cf. Ellis and Dunlap, 1988).

Initial fault propagation may have been low relative to slip rate, or the fault tip may have been pinned as fault slip increased (McConnell et al., 1997). These conditions would continue to favor fold growth in B-3. Observations of synform development (Fig. 7) fit the conceptional model of McConnell et al. (1997) for fold growth below a pinned thrust tip. The underlying mica schist layer presumably was incompetent enough to be evacuated by synformal growth into the adjacent antiformal core.

On the basis of these relations, we suggest that the following steps had occurred by the end of B-3: deflection-driven folding prior to thrusting, thrust nucleation as a result of stretching and competency contrasts, and subsequent fold growth at the pinned thrust tip (Fig. 10). The sequence of events is more plausible than an interpretation of thrusting related to strain hardening as a result of fold tightening; there were no continuous fold limbs to tighten since the gash fracture disrupted the continuity of migmatitic schist layering.

Antiforms in the early B-series structures have moderately inclined profiles (Figs. 6 and 7). A line drawn upward along the axial surface of the synform, through the center of the gash fracture, and then outward along the axial surface of the antiform has a smoothly curving S-shape. The curving shape suggests that flattening occurred away from the steeper part of the line defined by the gash fracture. The line also implies rotation toward a more recumbent profile. Rotation has the same sense of slip as the fault (Cooke and Pollard, 1997). That is, the antiform flattened to the west, and the synform flattened to the east. In a model of fault-related folds in the southeast Pyrenees, synclinal axial surfaces resulting from trishear are concave upward (Ford et al., 1997). This fold form is the result of deformation about a hinterland pinpoint and ongoing deformation throughout the synform, so that as the fold pair grew, the synform became progressively overturned and strained (Ford et al., 1997).

A small thrust occurs near the base of B-3 (Fig. 7). Although a basal detachment is not exposed, this thrust is considered to be an imbricate splay of that detachment. The thrust has begun to cut the antiformal forelimb near the hinge zone of the synform. This thrust has the characteristics of a break-thrust (Woodward, 1997). Any additional, up-section thrust propagation should be expected to follow the S-shape of our imaginary curving line. Thrusting through or just above the synform's hinge would leave only part of the trough.

The point of highest strain, however, might be expected to control any up-section propagation. Once the thrust broke through the synform, the point of highest strain would be the tip of the down-section propagating thrust (Fig. 7). A stress concentration at the down-section thrust tip would deflect the up-section thrust from the axial surface of the synform and 'captured' movement. Capture would link the two approaching thrust tips and create a thrust ramp. Subsequent thrusting through the points of highest strain, i.e. steeper in the middle and flatter both up- and down-section, is consistent with Suppe's (1983) contention that a flat–ramp–flat fault shape is present prior to fault slip. Moreover, the inclinations of the axial surface of the flattened synform and of the downward propagating thrust adjacent to the gash fracture would determine thrust-ramp angle.

In summary, the early B-series defines a deformation progression leading from deflection of layer-parallel shortening to the connection of a down-section propagating thrust with a thrust splay of a basal detachment that forms a thrust ramp. Other observations also show that the east-dipping orientation of the gash-fractures ultimately lead to ramp development. These three early stages clearly favor the Eisenstadt and DePaor (1987) model.

4.2. Later stages of development (B-4, B-5)

Once the fault tips linked, structural development during the two subsequent stages is considered to be controlled by upward movement on the throughgoing fault. Morley (1994) stated that, with upward movement, a new style of deformation can overprint the original one. Such overprinting could lead to a focus on the final structural style and little suspicion of an older deformation progression.

Observations of B-4 and B-5 do indicate a different style as compared with the older B-series structures (Figs. 5 and 6). Antiforms in both B-4 and B-5 have angular hinges as compared with earlier rounded hinge zones. Folds with angular hinge zones are produced by kink-band folding, whereas folds with rounded hinge zones are produced by trishear (Ford et al., 1997). Also, localized slip on a few layers drives kink folding, whereas uniform slip on many layers leads to concentric folds (Woodward, 1997, and references therein).

The association of B-4 with the four structures preserved in the bench requires special explanation. No thrust is identified in the forelimb of the antiform, and gash fractures are absent. B-4 is placed in the progression because kinking was initiated at an intermediate stage of structural development. Kinking may have been the result of a change in the local strain path. Initiation of kinking does indicate that tri-shear processes became inactive in the intermediate stages of the progression.

The B-4 kink probably formed ahead of the blind, westward-propagating detachment—an imbricate splay of that detachment ramps out of the mica schist at B-5. We envision that kinking may have resulted as follows: westward-directed slip associated with the blind detachment encountered a small, backlimb antiform before the B-3-like, inclined fold pair. Localization on that antiform fixed the kink's synformal hinge near the adjacent antiform hinge zone.

Slickenlines on backlimb and forelimb layer boundaries of the fold indicate flexural slip during limb rotation. Flexural slip associated with kink folding produces angular hinge zones (Stewart and Alvarez, 1991). Early buckling of mica schist layers in the underlying synform probably ceased as flexural slip began, and the fold grew by limb rotation about fixed antiformal and synformal hinges (Fisher et al., 1992). Subsequent growth and rotation at a fixed, synformal inflection point enlarged the fold (Fig. 8). The 70° E-dipping forelimb of the fold also indicates that the forelimb is overturned. With continued shortening, progressive forelimb rotation formed

the angular hinge zone, tightened the fold, overturned the forelimb, and imparted the asymmetric profile.

We interpret that fold hinges were fixed by the presence of a minor fold on the backlimb of a larger structure. The upright, open antiform that lies 15 cm east of the B-3 thrust could represent such a structure (Fig. 7). Johnson (1977) points out that sinusoidal buckling precedes kink folding, that early buckling still may be reflected in kink geometry, and that the initial fold may be hardly developed when kinking begins. On the basis of these relations, we suggest that the antiform–synform pair on the chevron's forelimb is a relic of an older buckling event. We further suggest that a backlimb fold similar to the one in B-3 may have localized kinking.

In B-5, a thrust fault is subparallel with the gash fracture (Fig. 9). Initially, the thrust followed the synform's axial surface, and part of its trough is preserved in the footwall. The amount of reverse movement that occurred is uncertain as a result of thinning of the adjacent units.

Upward thrust movement on the ramp is interpreted to have initiated kink folding as slip was transferred from the fault tip (Figs. 9 and 10e). The faulted antiformal hinge at the migmatitic schist–mica schist contact defines this deformation. The backlimb of this fold is subhorizontal, and such an attitude suggests that backlimb rotation may have occurred (cf. Johnson, 1977). Backlimb rotation would have had an opposite slip direction (eastward) as flexural slip associated with kinking (westward) and would have returned the lithologic contact to a somewhat subhorizontal position (Johnson, 1977). Observations of D1 structures in the borrow pit show that contacts are subhorizontal (Clendenin and Garihan, 2004).

Adjacent to the B-5 gash fracture, migmatitic schist layers are folded into an asymmetric, east-dipping, moderately inclined, close synform (Fig. 9). This synform cannot be traced upward; a more open synform appears to overprint the close synform above the gash fracture-tip. We suggest that the overprinting represents refolding and a linear displacement by plastic yielding (Honea and Johnson, 1976). Kinking and plastic yielding above the gash fracture-tip also refolded the amphibolite–migamatitic schist contact and formed the angular hinge of the chevron.

In their study of the eastern Pyrenees, Suppe et al. (1997) modeled anticlinal hinge faulting as being episodic, sudden events that are independent or out-of-phase and related to kink-band migration. We believe that this idea can be applied to B-5. B-5 development likely was independent of footwall folding, as upward movement of the throughgoing fault drove the final stages of development (Fig. 10e). A sudden propagation of the thrust through the hinge of the hanging wall fold would have terminated structural development. Timing and extent of fault propagation are dependent on the mechanical stratigraphy (Mitra, 2002). Faulting, however, simply may have occurred to accommodate additional deformation (Erslev and Mayborn, 1997).

When the thrust broke through the hanging wall fold, flattening above the ramp would have occurred when the thrust encountered a higher detachment. Since mining already had removed rock above the bench, flattening was not observed. If a higher detachment was encountered above the amphibolite horizon, movement would have dissipated slip on the lower detachment and would have ended B-5 development.

B-4 and B-5 styles are in agreement with the Rich (1934) thrust model with the addition of kink folding (Fig. 10). The B-5 deformation path certainly appears to be controlled by upward movement on the throughgoing fault (cf. Morley, 1994; Mitra, 2002). If a thrust progressively transfers slip to kink folding developing at its tip, sudden changes in propagation versus slip relations of the fault would end localized folding, as slip was transferred to other zones. Such a relation suggests that faulting is the dominant deformation mechanism driving the later stages of structure development.

5. Conclusions

Field evidence from the Marietta borrow pit indicates that the three early stages of deflection-driven deformation favor the Eisenstadt and DePaor (1987) thrust model. The dominant deformation mechanism during those stages is folding and trishear. After the ramp is formed and upward movement is facilitated, the later two stages resemble the Rich (1934) thrust model. Then the dominant structural styles are kinking and faulting, with faulting or shear flow (B-4) being the driving mechanism.

The progressive overprinting of structural styles leads to a flat–ramp thrust geometry. Moreover, overprinting by younger, upward fault-driven structural styles tends to modify or mask older, footwall-fold dominated styles. These field relations show that development of fault-propagation folds may evolve through a number of episodic stages. One should be aware of the presence of competency contrasts, flaws, or other anisotropies capable of concentrating stress as stages of fault-propagation folding are interpreted.

Acknowledgements

We thank David Nix for access to the Lion Park Road borrow pit and logistical support. We also thank Malynn Fields for preparing the illustrations. Suggestions by David Lawrence and an anonymous reviewer greatly improved the manuscript. This project was funded in part by the South Carolina Department of Natural Resources and the Earth and Environmental Sciences Department at Furman University.

References

Alonso, J.L., Teixell, A., 1992. Forelimb deformation in some natural examples of fault-propagation folds. In: McClay, K.R. (Ed.), Thrust Tectonics. Chapman and Hall, London, pp. 175–180.

Bump, A.P., 2003. Reactivation, trishear modeling, and folded basement in Laramide uplifts: implications for the origins of intra-continental faults. GSA Today 13, 4–10.

Carreras, J., Druguet, E., Griera, A., 2005. Shear zone-related folds. Journal of Structural Geology 27, 1229–1251.

Clendenin, C.W., Garihan, J.M., 2004. Sequencing polyphase deformation within the Inner Piedmont: field evidence from near Marietta, South Carolina. South Carolina Geology 44, 1–12.

Cooke, M.L., Pollard, D.D., 1997. Bedding-plane slip in initial stages of fault-related folding. Journal of Structural Geology 19, 567–582.

Dixon, J.M., Liu, S., 1992. Centrifuge modeling of the propagation of thrust faults. In: McClay, K.R. (Ed.), Thrust Tectonics. Chapman and Hall, London, pp. 175–180.

Eisenstadt, G., DePaor, D.C., 1987. Alternative model of thrust fault propagation. Geology 15, 630–633.

Ellis, M.A., Dunlap, W.J., 1988. Displacement variation along thrust faults: implications for development of large thrusts. Journal of Structural Geology 10, 183–192.

Erslev, E.A., Mayborn, K.R., 1997. Multiple geometries and modes of fault-propagation folding in the Canadian thrust belt. Journal of Structural Geology 19, 321–335.

Fisher, M.P., Woodward, N.B., Mitchell, M.M., 1992. The kinematics of break-thrust folds. Journal of Structural Geology 14, 451–460.

Ford, M., Williams, E.A., Atoni, A., Verges, J., Hardy, S., 1997. Progressive evolution of a fault-related fold pair, from growth strata geometries Sant Llorenc de Morunys, SE Pyrenees. Journal of Structural Geology 19, 413–442.

Garihan, J.M., 2000. Geologic map of the Cleveland 7.5-minute quadrangle, Greenville and Pickens Counties, South Carolina. South Carolina Department of Natural Resources, Geological Survey Open File Report 130, scale 1:24,000.

Garihan, J.M., Ranson, W.A., Orlando, K.A., Preddy, M.S., 1990. Kinematic history of Mesozoic faults in northwest South Carolina. South Carolina Geology 33, 1–13.

Griffin Jr., V.S., 1974. Analysis of the Piedmont in northwest South Carolina. Geological Society of America Bulletin 85, 1123–1138.

Homza, T.X., Wallace, W.K., 1997. Detachment folds with fixed hinges and variable detachment depth, northeast Brooks Range, Alaska. Journal of Structural Geology 19, 337–354.

Honea, E., Johnson, A.M., 1976. Part IV. Development of sinusoidal and kink folds in multilayers confined by rigid boundaries. Tectonophysics 30, 197–239.

Johnson, A.M., 1977. Styles of Folding. Elsevier, New York.

Koyi, H.A., Sans, M., Teixell, A., Cotton, J., Zeyen, H., 2004. The significance of penetrative strain in the restoration of shortened layers—insights from Sand models and the Spanish Pyrenees. In: McClay, K.R. (Ed.), Thrust Tectonics and Hydrocarbon Systems. American Association Petroleum Geologists, Tulsa, pp. 207–222.

Liu, S., Dixon, J.M., 1995. Localization of duplex thrust-ramps by buckling: analog and numerical modeling. Journal of Structural Geology 17, 875–886.

McConnell, D.A., Katternhorn, S.A., Benner, L.M., 1997. Distribution of fault slip in outcrop-scale fault-related folds, Appalachian Mountains. Journal of Structural Geology 19, 257–268.

Mitra, S., 2002. Structural models of faulted detachment folds. American Association Petroleum Geologists Bulletin 86, 1673–1694.

Morley, C.K., 1994. Fold-generated imbricates: examples from the Caledonides of Southern Norway. Journal of Structural Geology 19, 619–632.

Passchier, C.W., Trouw, R.A.J., 1998. Microtectonics. Springer, Berlin.

Ramsay, J.G., 1992. Some geometric problems of ramp-thrust models. In: McClay, K.R. (Ed.), Thrust Tectonics. Chapman and Hall, London, pp. 191–200.

Rich, J.L., 1934. Mechanics of low-angle overthrust faulting as illustrated by Cumberland thrust block, Virginia, Kentucky, and Tennessee. American Association Petroleum Geologists Bulletin 18, 1584–1587.

Stewart, K.G., Alvarez, W., 1991. Mobile-hinge kinking in layered rocks and models. Journal of Structural Geology 13, 243–260.

Storti, F., Salvini, F., McClay, K., 1997. Fault-related folding in sandbox analogue models of thrust wedges. Journal of Structural Geology 19, 583–602.

Suppe, J., 1983. Geometry and kinematics of fault-bend folding. American Journal of Science 283, 684–721.

Suppe, J., Sabat, J., Munoz, J.A., Poblet, J., Roca, E., Verges, J., 1997. Bed-by-bed fold growth by kink-band migration: Sant Llorenc de Morunys, eastern Pyrenees. Journal of Structural Geology 19, 443–462.

Woodward, N.B., 1997. Low-amplitude evolution of break-thrust folding. Journal of Structural Geology 19, 293–302.